Journal of Solid State Chemistry 212 (2014) 92–98

Contents lists available at ScienceDirect

Journal of Solid State Chemistry

journal homepage: www.elsevier.com/locate/jssc

Electrochemical behavior of $[\{Mn(Bpy)\}(VO_3)_2] \approx (H_2O)_{1.24}$ and $[\{Mn(Bpy)_{0.5}\}(VO_3)_2] \approx (H_2O)_{0.62}$ inorganic–organic Brannerites in lithium and sodium cells

Roberto Fernández de Luis [a], Alexandre Ponrouch [b], M. Rosa Palacín [b], M. Karmele Urtiaga [a], María I. Arriortua [a,*]

[a] Departamento de Mineralogía y Petrología, Facultad de Ciencia y Tecnología, Universidad del País Vasco, UPV/EHU, Apdo. 644, E-48080 Bilbao, Spain
[b] Institut de Ciència de Materials de Barcelona (CSIC) Campus UAB, E-08193, Bellaterra, Catalonia, Spain

ARTICLE INFO

Article history:
Received 11 November 2013
Received in revised form
9 January 2014
Accepted 11 January 2014
Available online 18 January 2014

Keywords:
Electrode materials
Hybrid materials
Lithium batteries
Sodium batteries
Conversion reaction
Infrared spectroscopy

ABSTRACT

The performance of MnV_2O_6 (**MnV**) and its $[\{Mn(Bpy)\}(VO_3)_2] \approx (H_2O)_{1.16}$ (**MnBpy**) and $[\{Mn(Bpy)_{0.5}\}(VO_3)_2] \approx (H_2O)_{0.62}$ (**MnBpy0.5**) hybrid derivative compounds was investigated against sodium and lithium counter electrodes. For MnV_2O_6 stable capacities of 850 mAh/g were achieved in lithium cells, the best value reported so far. The whole capacity is ascribed to a conversion reaction in which the amorphization of the compounds takes place. No significant differences in the capacities for the inorganic compound and the hybrid ones were observed. Interestingly, the potential hysteresis decreases in the hybrid compounds. The difference between Li and Na cell capacity most probably comes from the difference of standard potential of the two redox couples Li^+/Li and Na^+/Na of about ca. 0.3 V leading to an incomplete conversion reaction and thus lowers capacity in the case of Na cells. The Raman and IR ex-situ experiments after cycling indicate that the bipyridine organic ligands are completely decomposed during the electrochemical testing. The IR studies in **MnV** inorganic and **MnBpy** and **MnBpy0.5** hybrid electrodes after the electrochemical cycling, suggest that the SEI formation and bipyridine degradation give rise to different aliphatic compounds.

1. Introduction

The development of new electrode materials with high capacity is one of the key issues for the development of high performance energy storage devices [1]. Within this scenario, the scientific community has begun to consider metal organic frameworks (MOFs), and inorganic–organic hybrid materials as candidates for positive and negative electrodes in Li-ion batteries [2]. Those compounds exhibit more open crystal architectures than the classical inorganic electrodes, in principle favoring the lithium insertion and diffusion processes. With regard to the positive electrode hybrid materials, several studies have been carried out with for instance Fe-MIL53 metal organic polymer [3], compounds having Prussian Blue crystal structure [4], and hybrid metal phosphates [5]. $Zn_4O(BTB)_2 \cdot (DEF)_m \cdot (H_2O)_n$ and $M_3(HCOO)_6$ (M=Zn, Co) MOFs have been considered for negative electrodes in lithium batteries, the later showing capacities as high as 560 mAh/g at C/9 [6]. In $Zn_4O(BTB)_2 \cdot (DEF)_m \cdot (H_2O)_n$ the capacity is achieved through a conversion reaction [7]. leading to the formation of Li_2O and reduction of the Zn to the metallic state at the end of discharge, whereas in the case of $M_3(HCOO)_6$ the formate ligand has an active and reversible role in the electrochemical mechanism, and Li(HCOO) compound is formed during the discharge.

Recently, we synthesized the hybrid inorganic–organic $[\{Mn(Bpy)\}(VO_3)_2] \approx (H_2O)_{1.16}$ **(MnBpy)** and $[\{Mn(Bpy)_{0.5}\}(VO_3)_2] \approx (H_2O)_{0.62}$ **(MnBpy0.5)** Brannerites (Bpy=4,4′-bipyridine), which crystal structures are closely related to that of the inorganic MnV_2O_6 **(MnV)** vanadate [8]. The use of the later as negative electrode for lithium batteries has been thoroughly studied during the last decades, showing stable capacities of around 650–750 mAh/g. These are ascribed to a conversion reaction leading to the amorphization of the MnV_2O_6 vanadate and reduction of Mn^{2+} to Mn(0) and of V^{5+} to V^{3+} [9]. In this work the electrochemical performances in Li and Na half cells and the ex-situ IR studies of the electrodes after electrochemical cycling of **MnV** and the hybrid **MnBpy** and **MnBpy0.5** Brannerites are presented. As far as we know, this is the first report on MnV_2O_6 or on inorganic–organic materials as electrodes material in Na-cells.

* Corresponding author. Tel.: +34 946012534; fax: +34 946013500.
E-mail addresses: roberto.fernandez@ehu.es (R. Fernández de Luis), aponrouch@icmab.es (A. Ponrouch), rosa.palacin@icmab.es (M. Rosa Palacín), karmele.urtiaga@ehu.es (M. Karmele Urtiaga), maribel.arriortua@ehu.es (M.I. Arriortua).

0022-4596/$ - see front matter © 2014 Elsevier Inc. All rights reserved.
http://dx.doi.org/10.1016/j.jssc.2014.01.013

2. Experimental

Commercially available reagent grade chemicals were purchased from Sigma-Aldrich. These were used without further purification. All synthetic reactions were carried out in 50 mL Parr Teflon-lined acid digestion bombs. The same synthesis pathway was used to prepare all the studied compounds. The reagents were mixed in 30 mL of distilled water under vigorous stirring. The pH value was adjusted with 1 M HNO_3 solution. Hydrothermal reactions have been carried out under slightly acidic (pH=6.5) and acidic conditions (pH=4.0). The mixtures were placed in 50-mL Parr Teflon lined autoclaves and heated at 170 °C for 3 days. After the reaction, the products were washed with distilled water and acetone, dried in air, and observed under a binocular microscope. The samples were also characterized by powder X-ray diffraction and IR spectroscopy. Many reactions with varying reaction conditions (stoichiometry, reaction time, temperatures, pH value, and concentrations) were studied in the $MnCl_2 \cdot 4H_2O/NaVO_3/4,4'$-Bipyridine (Bpy) system. The main results are plotted in compositional space diagrams and discussed in the Result and discussion section, focusing on the results obtained in the reactions carried out at 170 °C for 3 days.

2.1. Hydrothermal synthesis

Synthesis of **$[\{Mn(Bpy)\}(VO_3)_2] \approx (H_2O)_{1.16}$. (MnBpy)** Reagents: $NaVO_3$ (0.76 mmol), 4,4′-Bipyridine (2.27 mmol), $MnCl_2$ $4H_2O$ (2.27 mmol), and H_2O(40 mL). pH value: 6.0. After the reaction, orange microcrystalline phases together with a small amount of plate-like crystals of the same color are obtained. Synthesis of **$[\{Mn(Bpy)_{0.5}\}(VO_3)_2] \approx (H_2O)_{0.62}$. (MnBpy0.5).** The preparation of **MnBpy0.5** was similar to that of **MnBpy** except the pH was adjusted to 4.0. After the reactions, a significant amount of unreacted bipyridine was observed. In order to eliminate the excess of bipyridine organic ligand, the samples were dispersed in 30 mL of ethanol and sonicated for 10 min. The water was poured off after allowing the polycrystalline sample to settle. This process was repeated until pure samples were obtained, as judged by PXRD and visually under a microscope. Synthesis of **MnV_2O_6. (MnV)** Reagents: $NaVO_3$ (0.67 mmol), 4,4′-Bipyridine (2.01 mmol), $MnCl_2$ $4H_2O$ (2.02 mmol), and H_2O (40 mL). pH value: 4.0.

2.2. Samples characterization

The percentage of the elements was calculated from atomic absorption spectroscopy (AAS) and C, N, H elemental analysis results. **MnBpy** Found: Mn, 12.71(2)%, V 23.52(2)%; C, 27.80 (2)%; N, 6.41(2)%; H, 2.35(3)%. **MnBpy0.5** Found: Mn, 16.11(2)%; V, 29.55 (3)%; C, 17.50(1)%; N, 4.08(1)%; H, 1.52(3)%. **MnV** Found: Mn, 21.58 (2)%, V 40.72(2)%.

The samples were characterized by X-ray powder diffraction data, recorded in a Philips X'Pert (CuKα) diffractometer (Cu$K\alpha 1$ radiation, 2θ range=5–70°, step size=0.015°, exposure time=10 s per step). The Rietveld and pattern matching refinements were carried out with the FULLPRORF software. [10] For **MnBpy**, the refinement shows the existence of an extra maxima at 2θ=28.2° related to the existence of a minor proportion (≈ 1%) unidentified impurity (χ^2=2.84, R_B=12.1, R_p=26.4, R_{exp}=19.76). The Rietveld refinement for **MnBpy05**, gives rise to a very poor fit due to the strong preferred orientation of the {00l} family of reflexions. In order to corroborate the purity of the sample the pattern matching analysis was carried out for **MnBpy05**. The final fit shows a very good agreement with the initial monoclinic cell (χ^2=3.56, R_B=1.04, R_p=10.1, R_{exp}=6.98). For **MnV**, the final agreement factors for the Rietveld refinement are χ^2=2.29, R_B=13.7, R_p= 16.5, R_{exp}=14.75. Patterns of the un-cycled electrodes were also recorded in the same conditions for the sake of comparison. As judged by PXRD, in the tapes casted electrodes the active materials remains unchanged (Fig. S1).

2.3. Electrochemistry

Electrochemical tests were performed in two-electrode Swagelok cells [11] using lithium or sodium metal (Aldrich, 99.9%) as counter and reference electrodes. The working electrodes consist of a tape casted electrode prepared following a procedure described elsewhere [12]. Briefly, 65% of active material, 27% of carbon black (Super P, Timcal, Bodio, Switzerland), and 8% of polyvinylidene fluoride (PVDF; Arkema, Colombes, France) binder and *N*-Methylpyrrolidone (NMP, Aldrich) were ball milled (stainless steel container, 3 stainless steel balls of 1 cm diameter, 500 rpm, 1 h) using a PM100 Retsch planetary Ball Miller. The slurry was tape casted on a 20 μm thick copper foil (Goodfellow Huntingdon, UK) using a 250 μm Doctor-Blade and further dried at 120 °C under vacuum. Disk working electrodes (0.8 cm^2) were cut from the tape and pressed at 8 t during 1 min. Two sheets of GF/D borosilicate glass fiber (Whatman, Kent, UK) were used as separator, soaked with 0.5 cm^3 of electrolyte. 1 M hexafluoorphosphate ($LiPF_6$) in dimethyl carbonate:ethylene carbonate (1:1) electrolyte (LP30, Merck) were used in the case of lithium cells, while 1 M $NaClO_4$ (Aldrich, 98%) in $EC_{0.45}$:$PC_{0.45}$:$DMC_{0.1}$ was used as electrolyte [13]. Electrochemical tests were performed using a Bio-Logic VMP3 potentiostat through galvanostatic cycling with potential limitation (GCPL) experiments. The voltage window was 0.01–3 V and the rate was varied from C/20 to C (C 1 being one Li^+ or Na^+ inserted in one hour).

2.4. IR and Raman spectroscopy

After cycling the cells were stopped in the fully discharged state and dismantled inside an argon filled glove box. The working electrodes were then rinsed with DMC. The IR, Raman analyses were performed on the cycled working electrodes. Measurements were also carried out on un-cycled electrodes for the sake of comparison. The samples were transported in vacuum, minimizing, as much as possible, their exposure to air. The IR spectra were recorded on a Jasco FT/IR-6100 spectrometer with pressed KBr pellets (400–4000 cm^{-1}). Raman spectra were measured on a Ranishaw Raman confocal microscopy spectrophotometer using the 514 nm laser line for excitation.

2.5. Electron microscopy

The morphology of the as-synthesized samples was examined with a JEOL JSM-7000F scanning electron microscope (SEM) equipped with a Schottky field emission gun (FEG) and an Oxford Inca Pentafet X3 energy dispersive X-ray analyzer (EDX).

3. Results and discussion

3.1. Hydrothermal synthesis

The compositional space diagrams constructed from the hydrothermal reactions carried out with different initial stoichiometries at pH=6.5 and 4.0 are shown in the Fig. 1. At slightly acidic conditions (Fig. 1(a)) the three main crystallization fields are associated with the MnV_2O_6 and $Mn_2V_2O_7$ inorganic vanadates and the $[\{Mn(Bpy)\}(VO_3)_2] \cdot 1.2H_2O$ hybrid compound. When the pH is reduced to 4.0 the $[\{Mn(Bpy)_{0.5}\}(VO_3)_2] \cdot 1.2H_2O$ hybrid vanadate crystallizes instead of the $[\{Mn(Bpy)\}(VO_3)_2] \cdot 1.2H_2O$ phase, obtained at slightly acidic conditions (Fig. 1(b)). So, the

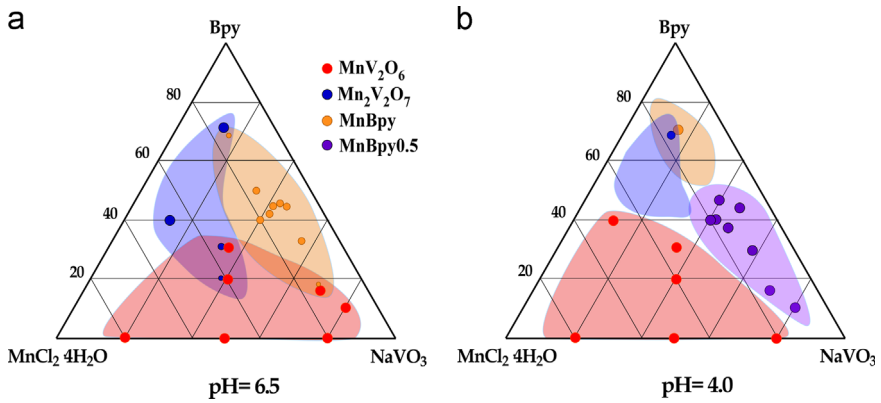

Fig. 1. Compositional space diagrams for the $MnCl_2 \cdot 6H_2O/NaVO_3$/bipyridine system for (a) ph=6.5 and (b) pH 4.0.

crystallization of the hybrid Brannerites depends on the acidity of the media, and it is favored by initial stoichiometries rich in $NaVO_3$ and bipyridine. The concentration of the system is also crucial for obtaining the hybrid Brannerites. With the same 1:3:3 initial molar relation of reagents, but lower concentration, inorganic $Mn_2V_2O_7$ and MnV_2O_6 vanadates are obtained instead of the hybrid compounds. (Fig. S.2) The MnV_2O_6 inorganic Brannerite crystallization is favored by acidic conditions and reducing or suppressing the presence of bipyridine in the reaction media.

It is well known that, among other variables, the stability in solution of one vanadate species over another strongly depends on the pH and vanadium concentration of the media [14]. In the concrete case of the studied system, the pH of the media does not affect the vanadium oxide subunit present in the crystal structures, but influences the content of bipyridine. Previous studies show that, for nickel hybrid vanadates, the compounds obtained at neutral or slightly acidic conditions possess more open crystal structures and greater content of organic ligand than those crystallized at acidic conditions [15].

After the hydrothermal synthesis, the particle size and morphology of the samples were studied by binocular microscope and electron microscopy. The Fig. S.3 shows the morphology of the as-synthesized **MnBpy**, **MnBpy0.5** and **MnV** samples. For **MnV,** the plates like crystals are agglomerated in micrometric gypsum-like flowers. The thickness of the individual plates is approximately of 0.1 μm. The **MnBpy** and **MnBpy0.5** phases crystallized as well defined single crystals. In the specific case of **MnBpy0.5** the size of the prismatic single crystals is micrometric. The **MnBpy** plate like single crystals are also agglomerated in gypsum-like flower morphology and each individual single crystal possess plate like morphology similar to those of **MnV** phase.

3.2. Crystal Structures

The crystal structures of the inorganic and inorganic–organic Brannerites have been previously reported (see Ref. [8,9] Briefly, all the crystal structures are three dimensional architectures constructed from two common structural building blocks: edge shared manganese octahedra chains and edge shared VO_5 polyhedral zigzag chains (Fig. 2). In the specific case of hybrid vanadates, the bipyridine organic ligand is incorporated into the crystal structures. The crystal framework of **MnBpy** is formed from inorganic layers pillared by the organic ligand. The manganese chains are linked through the metavanadate chains. The connectivity of the structural units generates [010] inter-layer channels, in which the disordered crystallization water molecules are located. The terminal oxygen atoms belonging to the double metavanadate chains point towards the center of the [010] channels (Fig. 2(a)). In **MnBpy0.5** the linkage of two single inorganic layers, related by a center of symmetry, generates double inorganic layers. Those layers possess inorganic intralayer channels composed of six polyhedra. The double layers are pillared by the bipyridine organic ligand giving rise also to [010] interlayer channels in which are located the crystallization water molecules (Fig. 2(b)). In the MnV_2O_6 inorganic Brannerite, the double metavanadate chains links four manganese chains, and each chain of edge shared manganese octahedra connects also four double metavanadate chains, forming a three dimensional inorganic framework (Fig. 2(c)). The six polyhedral channels in **MnV** are more compressed than those intralayer channels observed in **MnBpy0.5**.

If we take into account the crystal structures of the hybrid compound two possible Li^+ or Na^+ insertion pathways can be identified. The interlayer channels in which are located crystallization water molecules are large enough to allow insertion/deinsertion processes. In the specific case of the **MnBpy0.5** compound the intralayer [010] six polyhedral channels are also possible migration pathways for mobile cations. But the question arises in if the cations of the hybrid compounds could adopt different oxidation states without inducing the crystal structure collapse. In that regard, the most likely oxidation state change could be related to the V^{5+}/V^{4+} redox couple, because both the V^{5+} and V^{4+} oxidation states can adopt five coordination environments with similar V–O bond distances.

3.3. Electrochemical measurements

Among the alternatives to commercially used graphitic carbon for negative electrode materials in lithium batteries, materials operating through conversion reaction are interesting candidates and present very high specific capacity values [7]. In particular, MnV_2O_6 Brannerite has been shown to exhibit capacities as high as ca. 800 $mAhg^{-1}$, at 0.15C and good cyclability.

Some general trends can be deduced from electrochemical results reported by several research groups on MnV_2O_6 vanadates synthesized by different routes (ceramic, sol–gel, hydrothermal). The capacities achieved upon the first reduction are larger than those observed upon the first oxidation and subsequent cycles, which has been related to the degradation of the electrolyte [16]. The first reduction usually shows two pseudo-plateaus, the first at ca. 2.4 V vs. Li^+/Li^0, and the second one at 0.7 V vs. Li^+/Li^0, but the first one is not observed in all the reported studies. In-situ X-Ray diffraction experiments prove that MnV_2O_6 is stable in electrodes charged up to cut-off voltages of 1.0 V, and the diffraction maxima show progressive loss of intensity when the electrode is reduced to 0.7 V, disappearing completely at 0.4 V vs. Li^+/Li^0. Hara et al. proposed the amorphization of the MnV_2O_6 compound through a conversion to $Li_3MnV_2O_6$ rock-salt type structure compound [17].

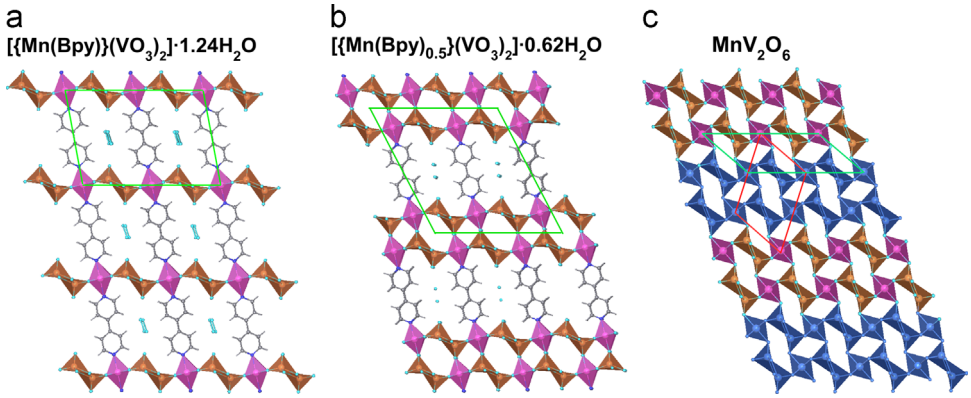

Fig. 2. Three dimensional crystal structures for **MnBpy** (a), **MnBpy0.5** (b) and **MnV** (c) compounds.

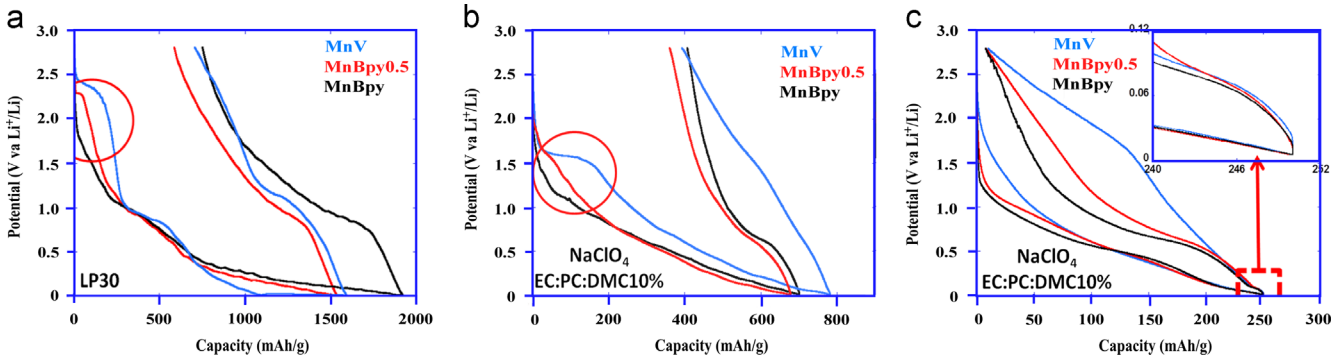

Fig. 3. First cycle potential vs. capacity profiles for **MnV** (blue curves), **MnBpy0.5** (red curves) and **MnBpy** (black curves) cycled against lithium (a) or sodium (b) counter electrodes at C/20. (c) Potential vs. normalized capacity profiles for the same half cells cycled at C/5 is presented in (b). (For interpretation of the references to color in this figure legend, the reader is referred to the web version of this article.)

The in-situ XFAS and XANES studies reveal that the oxidation state for the vanadium atoms is reduced from 5^+ to 3^+, and the Mn^{2+} is reduced to metallic Mn(0), during the first reduction, and are re-oxidized to V^{5+} and Mn^{2+} during the oxidation. All this facts are in good agreement with a conversion reaction mechanism in which the MnV_2O_6 Brannerite reacts at potentials lower than 0.7 V vs. Li^+/Li^0, giving rise to a Li_2O matrix surrounding the Mn(0) and V_xO_y nano-particles.

Fig. 3 shows the first cycle potential vs. capacity profiles for the **MnV** inorganic Brannerite and the **MnBpy0.5** and **MnBpy** hybrid vanadates cycled against lithium (Fig. 3(a)) and sodium (Fig. 3(b)) counter electrodes. Two plateaus between 2.4 and at 0.7 V vs. Li^+/Li, are observed upon reduction for **MnV**. Similar features are observed using sodium counter electrodes with a plateau being observed at ca. 1.7 V vs. Na^+/Na (cf. Fig. 3b, blue curve).

The first plateau at 2.4 V is not systematically observed in the previous studies on MnV_2O_6 inorganic brannerite and is most probably related to the synthetic conditions. Indeed, Morishita et al. [18] synthesized MnV_2O_6 using two different routes, and the first plateau is only observed in one of them. The studies carried out by Hara et al. indicate that the crystal structure of the **MnV** is stable down to 0.7 V, and no displacement in the diffraction maxima is observed during the first plateau, suggesting that there is no reversible lithium insertion into the crystal structure of **MnV**. In our measurements, the initial plateau gradually disappears when increasing the bipyridine content of the hybrid phases (cf. Fig. 3, red circles).

Upon the first reduction against lithium counter electrodes a slight increase in capacity was recorded at low potential (i.e. lower than 0.5 V vs. Li^+/Li) for hybrids **MnBpy** and **MnBpy0.5** when compared to **MnV** (cf. Fig. 3a). This phenomenon could possibly be ascribed to the reduction of the organic compound since the capacity related to this process is proportional to the organic content of the hybrid material (ca. 1260 mAh/g and 920 mAh/g, respectively, for **MnBpy** and **MnBpy0.5).** In contrast, similar profiles at low potentials were observed for **MnBpy**, **MnBpy0.5** and **MnV** in experiments with sodium counter electrodes. This is most probably due to the shift in potential when going from lithium to sodium cells (about 0.3 V) and these processes taking place below the low cut off potential and hence not observed. This shift in potential has a strong impact on the reversible capacity recorded upon cycling when comparing cells using lithium and sodium counter electrodes. Indeed, reversible capacities of ca. 850 and 300 mAh/g were recorded at C/20 for the **MnV** compound cycled, respectively, against lithium and sodium (cf. Fig. 4b), suggesting an incomplete conversion reaction in the latter case. The theoretical capacity for these compounds depends on the conversion mechanisms, the most plausible ones being:

$$\text{I}: \quad MnV_2O_6 + 6Li^+ + 6e^- \leftrightarrow Mn(0) + V_2O_3 + 3Li_2O$$
(theoretical capacity : 636 mAh/g)

$$\text{II}: \quad MnV_2O_6 + 8Li^+ + 8e^- \leftrightarrow Mn(0) + 2VO + 4Li_2O$$
(theoretical capacity : 848 mAh/g)

$$\text{III}: \quad MnV_2O_6 + 12Li^+ + 12e^- \leftrightarrow Mn(0) + 2V + 6Li_2O$$
(theoretical capacity : 1272 mAh/g)

The reversible capacity recorded upon cycling does not seem to be affected by the presence of bipyridine and similar values are recorded for **MnBpy**, **MnBpy0.5** and **MnV** (cf. Fig. 4a) but significant differences in the potential hysteresis between reduction and oxidation are observed. Indeed, it is found to decrease when going from the pure inorganic compound **MnV** to **MnBpy**

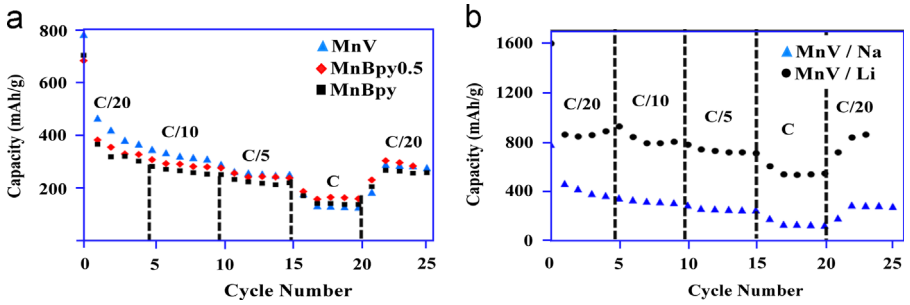

Fig. 4. Capacity upon reduction vs. cycle number for (a) **MnV**, **MnBpy0.5** and **MnBpy** cycled against sodium counter electrodes cells and (b) **MnV** cycled against lithium (electrolyte: LP30) or sodium (electrolyte: 1 M $NaClO_4$ in $EC_{0.45}$:$PC_{0.45}$:$DMC_{0.1}$) counter electrodes.

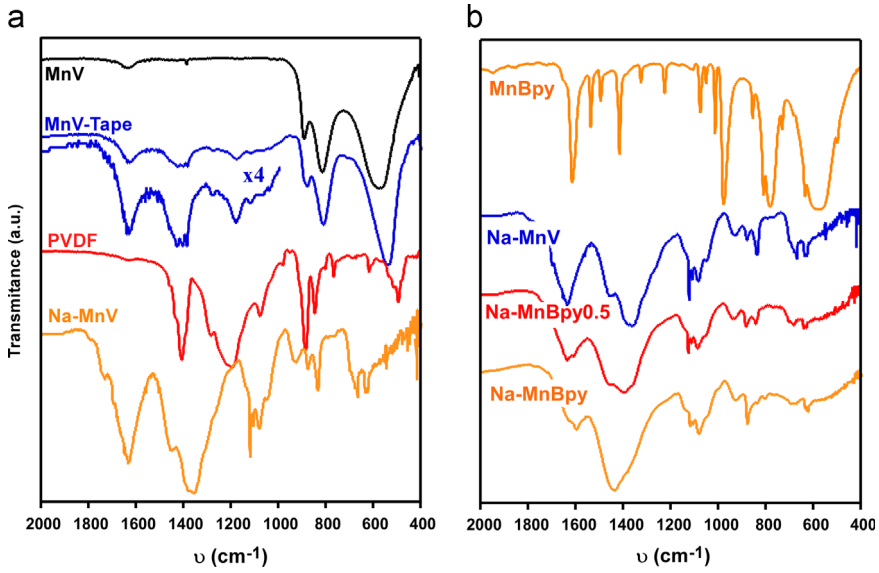

Fig. 5. (a) IR spectra of **MnV**, **MnV** Tape casted electrode before and after cycling in Na cells and PVDF (b) IR spectra of **MnV**, **MnBpy** and **MnBpy0.5** electrodes after cycling in Na cells. IR spectrum of the pristine **MnBpy** has been plotted for comparison.

(cf. Fig. 3a and b), the trend being more pronounced for the cells using sodium counter electrodes as seen from the potential versus normalized capacity profiles (cf. Fig. 3c). Interestingly, only the potential hysteresis is modified by the addition of bipyridine while similar values of coulombic efficiency (ca. 98.5%), discharge capacity (ca. 250 mAh/g) and IR drop between charge and discharge (ca. 10 mV, see inset in Fig. 3c) are recorded in all cases.

Fig. 4 displays the plots of the capacity versus the number of cycles calculated for **MnBpy**, **MnBpy0.5** and **MnV** tape casted electrodes cycled at various C rates ranging from C/20 up to 1C. Similar capacity values were recorded for **MnBpy**, **MnBpy0.5** and **MnV** based electrodes. For instance, stable capacity values were recorded after about 5 cycles for the cells using sodium counter electrodes and capacity values ranging from ca. 140 mAh/g (at 1C) up to ca. 300 mAh/g (at C/20) were calculated (cf. Fig. 4a). As already mentioned, much higher capacity values were obtained in the case of the cells using lithium counter electrodes with capacity as high as ca. 850 mAh/g recorded at C/20 together with good rate capability (ca. 540 mAh/g at 1C) (cf. Fig. 4b). To the best of our knowledge these are the highest capacity values and rate capability performances reported for the MnV_2O_6 vanadate.

3.4. Raman and IR studies of the initial samples and after electrochemical cycling in Li and Na cells

The IR and Raman spectra of the as-synthesized compounds are very similar (Fig. S4). Three main regions can be distinguished: (i) the absorption maxima related to the crystallization and coordinated water molecules (3700–3000 cm^{-1}), (ii) the bipyridine ligand vibrational modes generating absorption maxima in the 1700–1000 cm^{-1} range, and (iii) the absorption bands located at frequencies below 1000 cm^{-1}, associated to (V_4O_{12}) cycles, and tentatively assigned to the V=O streching (1000–900 cm^{-1}), $V_{as}(VO_4)^{-3}$ (890s cm^{-1}) and V_{as}(V–O–M) 725(s) vibrations. In the Raman spectra, the low Raman shift interval (600–140 cm^{-1}) contains also the vibrational information about the Mn–O and Mn–py and M–H_2O bonds. [19].

As expected, the signals of the absorption maxima related to the bipyridine ligand are stronger for **MnBpy** compound, in comparison with those of **MnV** inorganic vanadate. The main differences in the Raman spectra are observed in the interval associated to the vanadate units. Despite the crystal structures of **MnV**, **MnBpy** and **MnBpy0.5** are similar, the Raman shift associated to the V=O terminal groups are different. Indeed, the inorganic compound **MnV** and the hybrid **MnBpy** phase possess only one single signal for the V=O vibrational mode, while the **MnBpy0.5** phase possess two peaks. The intensity of the maxima associated to the $\upsilon_{as}(VO_5)$ vibrational mode decrease progressively with the organic content of the compounds. Slight differences are observed in the position and intensity of the maxima associated with the V–O_2 scissoring, υ(Mn–N), υ(Mn–O), υ(V–O) vibrational modes, and the deformation and torsional modes of the metavanadate chains. These observations are in good agreement with the slight differences of the structural building blocks and the V–O,

Mn–O and Mn–N bond distances in the **MnV**, **MnBpy0.5** and **MnBpy** crystal structures.

The IR spectra of the PVDF and those of the tape casted samples were recorded for sake of comparison with the IR spectra of the electrodes cycled against sodium. The main bands for PVDF IR spectra are located at 1400, 1284, 1200, 880 and 850 cm^{-1}, and are associated with different vibrational modes of the CF_2 and CH_2 groups (Fig. 5(a)). Despite the low weight percentage of PVDF (8%) in the electrodes, the absorption bands located at 1200 and 1400 cm^{-1} are clearly observed, while these at 880 and 850 are overlapped with the vibrational modes of the vanadate group. The IR spectra and the XRD patterns indicate that both the inorganic and organic compounds remain unchanged after the preparation of the electrodes (Figs. 5(a) and S1).

After cycling against sodium the absorption bands associated to the vanadate groups and bipyridine organic ligands disappear completely (Fig. 5(b)). The absence of vanadate group absorption bands is in good agreement with the proposed electrochemical conversion reaction from a 5^+ oxidation state to 2^+ one for the vanadium cations. The lack of second harmonic absorption maxima related to aromatic C–H groups (above 2000–1800 cm^{-1}) indicates the complete degradation of the pyridyl rings belonging to the bipyridine organic ligand.

Although the determination of bipyridine and electrolyte decomposition products is not trivial some general trends can be pointed out. First of all, the presence of medium intensity absorption maxima between 2960 and 2850 cm^{-1} are associated to the formation of compounds containing CH_3 and or CH_2 groups. These maxima are observed for **NaMnV**, **NaMnBpy** and **NaMnBpy0.5** cycled electrodes and are most probably associated with the formation of the SEI layer. Indeed, same main absorption bands are observed for **NaMnV**, **NaMnBpy** and **NaMnBpy0.5** cycled electrodes (1650, 1550–1300 and 1050 cm^{-1}) and in the previous works of Gachot et al. and Aroca et al. [20],which they ascribed to the vibrational modes of sodium alkoxides and carbonates [21].

In previous works, the electrolysis of pyridine in $AlCl_3$ solution was studies by Cisak and Elving [22]. These authors propose the formation of complex moistures of unsaturated polyanimes and polyamides during the reduction of pyridine. bipyridine clearly decompose upon cycling although its decomposition products cannot be identify unambiguously and have most probably similar IR signature than the electrolyte decomposition products.

4. Conclusions and discussion

The electrochemical performance comparison between the MnV_2O_6 inorganic brannerite and **MnBpy** and **MnBpy0.5** hybrid vanadates shows no differences in the capacity of the inorganic and hybrid phases. Based on the previous works in the MnV_2O_6 inorganic vanadate, the main capacity is ascribed to the conversion reaction of the active electrode through the reduction of V^{5+} to V^{3+} and Mn^{2+} to metallic Mn(0). For lithium cell, after the first reduction, capacities of 850 mAh/g (C/20) are reached for the **MnV** compound, which is, to the best of our knowledge, the highest value reported for the MnV_2O_6 vanadate. A significant decrease of the potential hysteresis between reduction and oxidation was observed when going from purely inorganic (i.e. **MnV**) to hybridized (i.e. **MnBpy0.5** and **MnBpy**) compounds. The ex-situ Raman and IR studies corroborate that the bipyridine ligand is completely decomposed during the electrochemical cycling, suggesting that the crystal structure of the hybrid compounds collapse. As judged by IR, and based on previous studies carried out on lithium cells, both SEI formation and the bipyridine reduction generate carbonates and aliphatic compounds.

Acknowledgments

This work has been financially supported by the Ministerio de Ciencia e Innovación (MAT2010-15375 and MAT2011-24757) and the Gobierno Vasco (IT-177-07), which we gratefully acknowledge. The authors thank the technicians of SGIker (UPV/EHU), Drs. J. Sangüesa, A. Larrañaga, P. Vitoria and I. Orue, financed by the National Program for the Promotion of Human Resources within the National Plan of Scientific Research, Development and Innovation, Ministerio de Ciencia y Tecnología and "Fondo Social Europeo" (FSE), for the X-ray diffraction and magnetic measurements, respectively. R. Fernández de Luis thanks to the MICINN (Madrid, Spain) (BES-2005-10322). E.S. Larrea thanks the UPV/EHU for funding.

Appendix A. Supporting information

Supplementary data associated with this article can be found in the online version at http://dx.doi.org/10.1016/j.jssc.2014.01.013.

References

[1] (a) J.B. Goodenough, Y. Kim, Chem. Mater. 22 (2010) 587–603;
(b) V. Etacheri, R. Maron, R. Elazari, G. Salitra, D. Aurbach, Energy Environ. Sci 4 (2011) 3243–3262;
(c) M.R. Palacín, Chem. Soc. Rev. 38 (2009) 2565–2575;
(d) V. Palomares, P. Serras, I. Villaluenga, K.B. Hueso, J. Carretero-González, T. Rojo, Energy Environ. Sci. 5 (2012) 5884–5901.
[2] A. Morozan, F. Jaouen, Energy Environ. Sci. 5 (2012) 9269–9290.
[3] (a) G. Férey, F. Millange, M. Morcrette, C. Serre, M.-L. Doublet, J.-M. Grenèche, J.-M. Tarascon, Angew. Chem. Int. Ed. 46 (2007) 3259–3263;
(b) G. de Combarieu, M. Morcrette, F. Millange, N. Guillou, J. Cabana, C.P. Grey, I. Margiolaki, G. Férey, J.-M. Tarascon, Chem. Mater. 21 (2009) 1602–1611;
(c) G. deCombarieu, S. Hamelet, F. Millange, M. Morcrette, J.-M. Tarascon, G. Férey, R.I. Walton, Electrochem. Commun. 11 (2009) 1881–1884;
(d) A. Fateeva, P. Horcajada, T. Devic, C. Serre, J. Marrot, J.-M. Grenèche, M. Morcrette, J.-M. Tarascon, G. Maurin, G. Férey, Eur. J. Inorg. Chem. (2010) 3789–3794.
[4] (a) M. Okubo, D. Asakura, Y. Mizuno, J.-D. Kim, T. Mizokowa, T. Kudo, I. Honma, J. Phys. Chem. Lett. 1 (2010) 2063–2071;
(b) C.D. Wessells, S.V. Peddada, M.T. McDowell, R.A. Huggings, Y. Cui, J. Electrochem. Soc. 159 (2012) A98–A103.
[5] (a) M. Nagarathinam, K. Saravanan, E.J.H. Phua, M.V. Reddy, B.V.R. Chowdari, J.J. Vittal, Angew. Chem. Int. Ed. 124 (2012) 5968–5972;
(b) C.-Y. Cheng, S.-J. Fu, C.-J. Yang, W.-H. Chen, K.-J. Lin, G.-H. Lee, Y. Wang, Angew. Chem. Int. Ed. 42 (2003) 1937–1940;
(c) P. Tran-Van, K. Barthelet, M. Morcrette, M. Herlem, J.-M. Tarascon, A.K. Cheetham, G. Férey, J. New Mater. Electrochem. Syst. 6 (2003) 29–31.
[6] (a) K. Savaranan, M. Nagarathinam, P. Balaya, J.J. Vittal, J. Mater. Chem. 20 (2010) 8329–8335;
(b) X. Li, F. Cheng, S. Zhang, J. Chen, J. Power Sour. 160 (2006) 542–547.
[7] J. Cabana, L. Monconduit, D. Larcher, M.R. Palacín, Adv. Mater. 22 (2010) E170–E192.
[8] R. Fernández de Luis, M.K. Urtiaga, J.L. Mesa, K. Vidal, L. Lezama, T. Rojo, M.I. Arriortua, Chem. Mater. 22 (2010) 5543–5553.
[9] (a) S.-S. Kim, H. Ikuta, M. Wakihara, Solid State Ion. 139 (2001) 57–65;
(b) M. Inagaki, T. Morishita, M. Hirano, V. Gupta, T. Nakajima, Solid State Ion. 156 (2003) 275–282;
(c) T. Morishita, H. Konno, Y. Izumi, M. Inagaki, Solid State Ion. 177 (2006) 1347–1353;
(d) W. Huang, S. Gao, X. Ding, L. Jiang, M. Wei, J. Alloy Compd. 495 (2010) 185–188;
(e) S. Lei, K. Tang, Y. Jin, C. Chen, Nanotechnology 18 (2007) 175605 (7 pp.);
(f) D. Hara, J. Shirakawa, H. Ikuta, Y. Uchimoto, M. Wakihara, T. Miyanaga, I. Watanabe, J. Mater. Chem. 12 (2002) 3717–3722;
(g) E. Andrukaitis, J.P. Cooper, J.H. Smit, J. Power Sour. 54 (1995) 465–469.
[10] (a) FULLPROF98, Program for Rietveld Pattern Matching Analysis of Powder Patterns, Grenoble, 1998.;
(b) J. Rodriguez-Carvajal, Phys. B 192 (1993) 55–69.
[11] D. Guyomard, J.M. Tarascon, J. Electrochem. Soc. 26 (1992) 343–350.
[12] (a) A. Ponrouch, M.R. Palacín, J. Power Sour. 196 (2011) 9682–9688;
(b) A. Ponrouch, M.R. Palacín, J. Power Sour. 212 (2012) 233–246.
[13] (a) A. Ponrouch, E. Marchante, M. Courty, J.M. Tarascon, M.R. Palacín, Energy Environ. Sci. 5 (2012) 8572–8583;
(b) A. Ponrouch, R. Dedryvère, D. Monti, A.E. Demet, J.M. Ateba Mba, L. Croguennec, C. Masquelier, P. Johansson, M.R. Palacín, Energy Environ. Sci. 6 (2013) 2361–2369.

[14] (a) J. Livaje, Coordin. Chem. Rev. 178 (1998) 999–1018;
(b) L. Bouhedja, N. Steunou, J. Maquet, J. Livage, J. Solid State Chem. 162 (2001) 315–321;
(c) T. Chirayil, P.Y. Zavalij, M.S. Whittingham, Chem. Mater. 10 (1998) 2629–2640.
[15] (a) E.S. Larrea, R. Fernández de Luis, J.L. Mesa, J.L. Pizarro, M.K. Urtiaga, T. Rojo, M.I. Arriortua, in: O.L. Ortiz, L.D. Ramirez (Eds.), Coordination Polymers and Metal Organic Frameworks: Properties, Types and Applications, Nova Science Publisher Inc., New York, 2012, pp. 1–58 (Chapter 1);
(b) R. Fernández de Luis, M.K. Urtiaga, J.L. Mesa, T. Rojo, M.I. Arriortua, J. Alloys Compd. 480 (2008) 54–56;
(c) R. Fernández de Luis, J.L. Mesa, M.K. Urtiaga, E.S. Larrea, T. Rojo, M. I. Arriortua, Inorg. Chem. 51 (2012) 2130–2139.
[16] A. Ponrouch, P.-L. Taberna, P. Simon, M.R. Palacín, Electrochim. Acta 61 (2012) 13–18.
[17] D. Hara, H. Ikuta, Y. Uchimoto, M. Wakihara, J. Mater. Chem. 12 (2002) 2507–2512.
[18] T. Morishita, K. Nomura, T. Inamasu, M. Inagaki, Solid State Ion. 176 (2005) 2235–2241.
[19] (a) R.L. Frost, K.L. Erickson, M.L. Weier, O. Carmody, Spectrochim. ActaA 61 (2005) 829–834;
(b) H. Watanabe, Y. Okamoto, K. Furuya, A. Sakamoto, M. Tasumi, J. Phys. Chem. A 106 (2002) 3318–3324;
(c) K. Furuya, K. Kawato, H. Yokoyama, A. Sakamoto, H. Tasumi, J. Phys. Chem. A 107 (2003) 8251–8258;
(d) V.G. Zubkov, L.L. Surat, A.P. Tyutyunnik, I.F. Berger, N.V. Tarakina, B. V. Slobodin, M.V. Kuznetsov, T.A. Denisova, N.A. Zhuravlev, L. A. Perelyaeva, I.V. Baklanova, I.R. Shein, A.L. Ivanovskii, Phys. Rev. B 77 (2008) (174113-1–174113-14).
[20] (a) R. Aroca, M. Nazri, G.A. Nazri, A.J. Camargo, M. Trsic, J. Solut. Chem. 29 (2000) 1047–1060;
(b) G. Gachot, S. Grugeon, M. Armand, S. Pilard, P. Guenot, J.-M. Tarascon, S. Laruelle, J. Power Sour. 178 (2008) 409–421.
[21] S. Matsuta, T. Asada, K. Kitaura, J. Electrochem. Soc. 147 (2000) 1695–1702.
[22] A. Cisak, P.J. Elving, Electrochim. Acta 10 (1965) 935–946.